SPECTRAL CHARACTERISTICS AND CLASSIFICATION OF URBAN LAND-COVER BASED ON AIRBORN HYPERSPECTRAL DATA

Konomi Hara[1*], Wen Liu[2], Fumio Yamazaki[1], Kentaro Suzuki[1] and Yoshihisa Maruyama[1]

[1] Chiba University, 1-33 Yayoi-cho, Inage-ku, Chiba 263-8522, Japan,
x0t0236@students.chiba-u.jp; fumio.yamazaki@faculty.chiba-u.ac.jp;
kentaro_suzuki@chiba-u.jp; ymaruyam@tu.chiba-u.ac.jp
[2] Tokyo Institute of Technology, 4259-G3-2 Nagatsuta, Midori-ku, Yokohama 226-8502 Japan,
liu.w.ad@m.titech.ac. jp

*Corresponding author: x0t0236@students.chiba-u.jp

ABSTRACT

Hyperspectral remote sensing makes it possible to obtain detailed spectral information of surface objects. Using airborne hyperspectral (HS) data acquired over Houston, Texas, USA, provided by the 2013 IEEE data fusion contest, the spectral reflectance characteristics of surface materials were investigated. A multispectral (MS) image acquired by WorldView-2 satellite was also introduced and it was compared with the HS image. A field measurement using a handheld spectroradiometer (EKO MS-720) was also carried out by the present authors. The irradiances of surface materials obtained by the measurement were also compared with the digital numbers of the 144 HS bands. Finally supervised classification was conducted for the HS and MS data and their results were discussed.

Keywords: hyperspectral data, CASI-1500, WorldView-2, spectroradiometer, land cover classification

INTRODUCTION

Recent advancements of remote sensing technology have enabled fine identification of surface materials due to improved spatial, temporal and spectral resolutions of sensors. The improvement in spatial resolution of satellite optical sensors is most drastic and the resultant very high-resolution images are now widely available through Google Earth. Fine spatial-resolution also helps to identify detailed damage situation of urban areas due to natural disasters, e.g. earthquakes and hurricanes [1-4].

Urban environment is generally complicated, mixture of both natural land-cover (e.g. bare ground, water, vegetation) and man-made or impervious land-cover (e.g. roads, buildings). The distribution of land-cover classes is important for environmental management, disaster management and urban planning. There have been many researches focusing on the classification of vegetation in agricultural lands or forests. However, researches on the classification of man-made land-surfaces in urban areas are still limited due to their high complexity. Owing to the fine spectral resolution, hyperspectral remote sensing data have potential to classify artificial land-cover with different materials. Hyperspectral remote sensing technology has advanced significantly in the last few decades and its overview is provided in literature [5, 6]. Several airborne and spaceborne instruments with over 200 spectral bands have already been developed and actually in use. Since hyperspectral imaging provides many narrow-banded images simultaneously, the acquired data should be compared with the spectral reflectance characteristics of surface materials from spectral library or by field observation [7].

In this study, a fundamental study to classify urban land-cover and land-use was carried out using a dataset from the 2013 IEEE data fusion contest [8]. Firstly, the spectral characteristics for both natural surfaces and artificial structures are investigated using the airborne hyperspectral data covering a part of Houston, Texas, USA, and they are compared with the ground-based spectral observation results, conducted recently in Houston, Texas by the present authors. Supervised land-cover classification is then carried out for the hyperspectral data. In addition, land-cover classification is also conducted for a 8-band WorldView-2 image covering the same area and the result is compared with that from the hyperspectral data.

THE STUDY AREA AND IMAGERY DATA USED

The Data Fusion Technical Committee of the IEEE Geoscience and Remote Sensing Society (GRSS) conducts Data Fusion Contest in the recent years. The 2013 Contest involves two datasets – a hyperspectral image and a LiDAR derived Digital Surface Model (DSM), both at the same spatial resolution (2.5 m). The datasets were acquired over the University of Houston's campus and its neighboring urban area, Huston, Texas, USA [8]. In this paper, we use this hyperspectral image for investigating the capability of hyperspectral data for land cover classfication in urban areas.

Figure 1 shows the study area including the University of Houston's campus and the neighboring area. The airborne hyperspectral image was acquired on June 23, 2012 between the times 17:37:10 to 17:39:50 (UTC), by the NSF-funded Center for Airborne Laser Mapping (NCALM). Note that the local starndard time in Texas is UTC -6 hours, and thus the image was taken about 20 - 23 minutes before noon. CASI-1500 visible to near-infrared (VNIR) hyperspectral sensor [9, 10] was used for the aerial observation and the acquired image consists of 144 spectral bands (up to 288 bands) in the 380 nm to 1050 nm region, that has been calibrated to at-sensor spectral radiance units [8]. The average height of the sensor above ground was about 5,500 ft (1,676 m).

A multispectral image acquired by WorldView-2 (WV2) satellite on October 16, 2010 at 17:27:02 (UTC) was also introduced in this study (**Figure 1**) for the purpose of comparison with the hyperspectrl image. The WV2 imagery consists of a Panchromatic band (0.5 m resolution) and 8 multispectral (2.0 m resolution) in the 425 nm to 950 nm region. Considering the difference of spatial

Figure 1. The study area including the University of Houston campus and the neighboring urban area in Houston, Texas, USA and imaging areas of hyperspectral and multispectral data.

Figure 2. True color composites of the hyperspectral image (top) and the multispectral image (bottom) for the CASI-1500 imaging area. The red square shows the study area.

resolutions between the hyperspectral and multispectral datasets, pansharpening was not applied to the WV2 data. **Figure 2** compares these two imagery data for the CASI-1500 imaging area. Because of the cloud cover seen in the hyperspectral image, the area with the red square was selected for a detailed investigation. These true color plots were made by selecting each band (B, G, R) having the highest value at WorldView-2's relative response ([11] shown in **Figure 3**) for the hyperspectral data and B (band-2), G (band-3), and R (band-4) for the multispectral image

False color composite images (**Figure 4**) were also produced for the multispectral image (B: band-3, G: band-4, R: band-7) and for the hyperspectral image of the corresponding nearest bands (dotted lines in **Figure 3**). The false color composites showed that the a lot of vegetation, that is seen in red color, exists in the case study site.

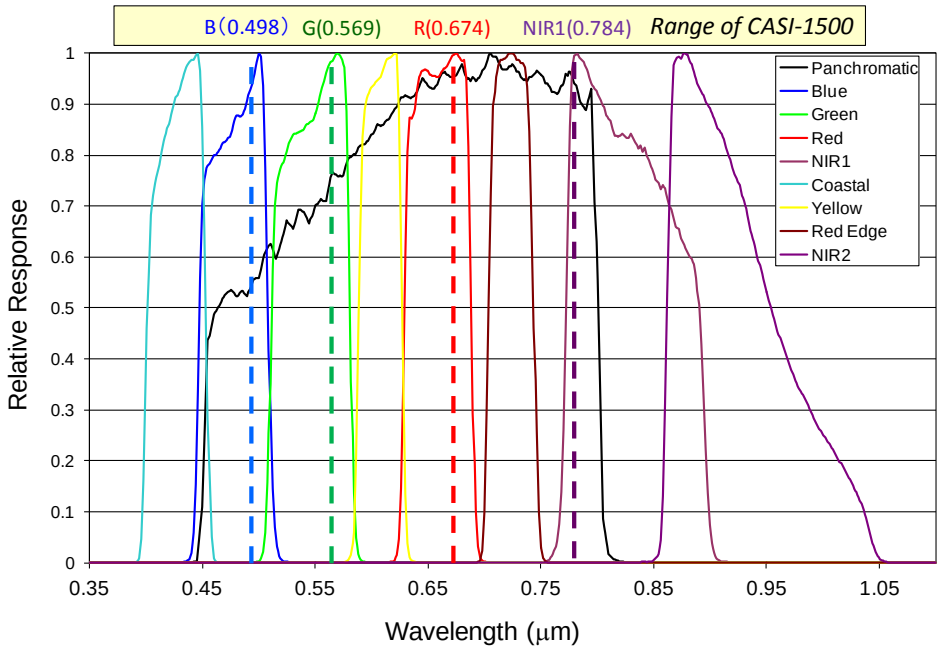

Figure 3. The relative spectral radiance response for WorldView-2 sensors [11] and the range of CASI-1500 hyperspectral sensor

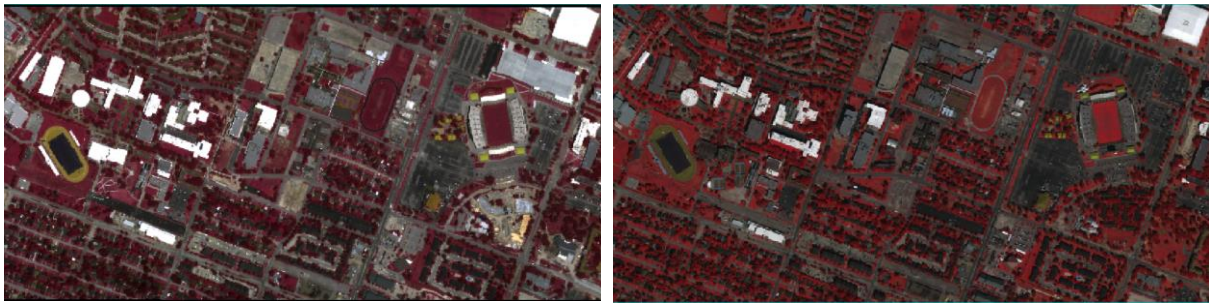

Figure 4. False color composites from the hyperspectral image (left) and multispectral image (right) corresponding to the red square in Figure 2

FIELD SURVEY AND SPECTRORADIOMETER OBSERVATION

In order to obtain ground truth data on spectroradiometric characteristics of surface materials in the study area, a field survey was conducted by the present authors on August 6th and 7th, 2013. A hand-held MS-720 spectroradiometer [12] made by EKO Instruments Co., Ltd., Japan was used. We have used this instrument for several years, e.g. to measure the health condition of tsunami-affected vegetation [13] and the irradiance of sunlit and shadowed Earth surfaces [14].

Figure 5 shows the field survey route by the present authors in the campus of Texas Southern University's football stadium and its surrounding area together with the locations and photos of three spectroradiometer observation points. The measurements were carried out in the times 15:45 to 16:45 (the local standard time: UTC -6) on August 6 and 10:00 to 10:40 on August 7, 2013. The weather was basically sunny but sometimes cloudy. We measured the irradiances of several surface materials in the study area and that of a white ceramic plate for reference. It is by no means easy to collect field data on the same time and date of spaceborne or airborne data acquisition. So we conducted the survey on the occasion of our trip to the USA, but the data we collected were almost in the same season (summer) with the hyperspectral image acquisition.

Figure 5. The field survey route (blue line) plotted on Google Erath by the present authors on August 6 and 7, 2013 in the campus of Texas Southern University's football stadium and its surrounding area, together with the locations and photos of three spectroradiometer observation points (a: lawn, b: artificial turf, c: concrete)

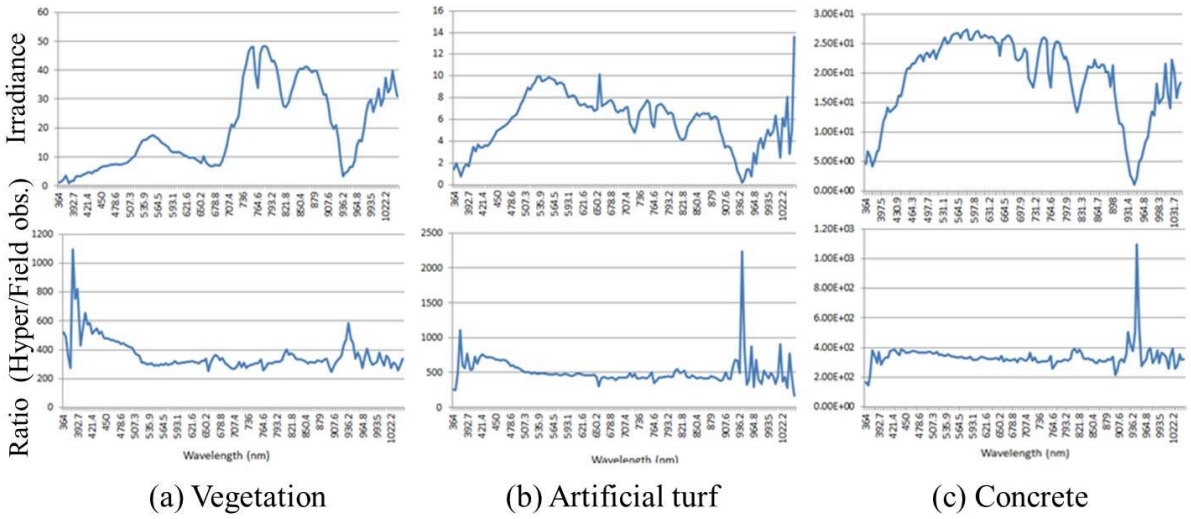

Figure 6. The observed irradiances of three surface materials (a: lawn, b: artificial turf, c: concrete) by our spectroradiometer field observation (top) and the spectral ratio between the hyperspectral image and the field observation data (bottom)

Figure 6 shows the observed irradiances of three surface materials (lawn, artificial turf, and concrete) by our spectroradiometer field measurement. In order to compare these results with the hyperspectral imagery data (DN: Digital Number), we plotted the irradiance values, instead of taking the irradiance ratio (reflectance) with respect to the white plate.

COMPARISON OF HYPERSPECTRAL AND MULTISPECTRAL IMAGES AND THEIR SUPERVISED CLASSIFICATION

Comparison of the hyperspectral (HS: CASI-1500) and multispectral (MS: WV-2) data was carried out the three surface materials (lawn, artificial turf, and concrete) shown in **Figure 5**. By extracting small areas (pixels) corresponding to these materials from the images, the averaged (with respect to pixels) digital numbers (DNs) are shown in **Figure 7** for the airborne (CASI-1500) and satellite (WV-2) sensors. Because the HS data have 144 bands, the DN values with respect to the wavelength look like the surface irradiance measured in the field (**Figure 6** top).

In order to compare the airborne hyperspectral data with the field spectroradiometer data, their spectral ratio (the airborne DN / the field irradiance) was calculated and shown also in **Figure 6** (bottom). Although the denominator (irradiance) and the numerator (DN) carry different units, the ratio is almost constant values with respect to the wavelength, for the three surface materials. A high peak (about 940 nm) seen in the ratio plot corresponds to the trough in the field observation data, due the atmospheric absorption effect caused by H_20 [6]. This observation supports that airborne hyperspectal sensing can provide the spectral reflectance characteristics of surface materials for a large imaging area, and thus it is quite useful to distinguish small change or difference in surface materials/conditions.

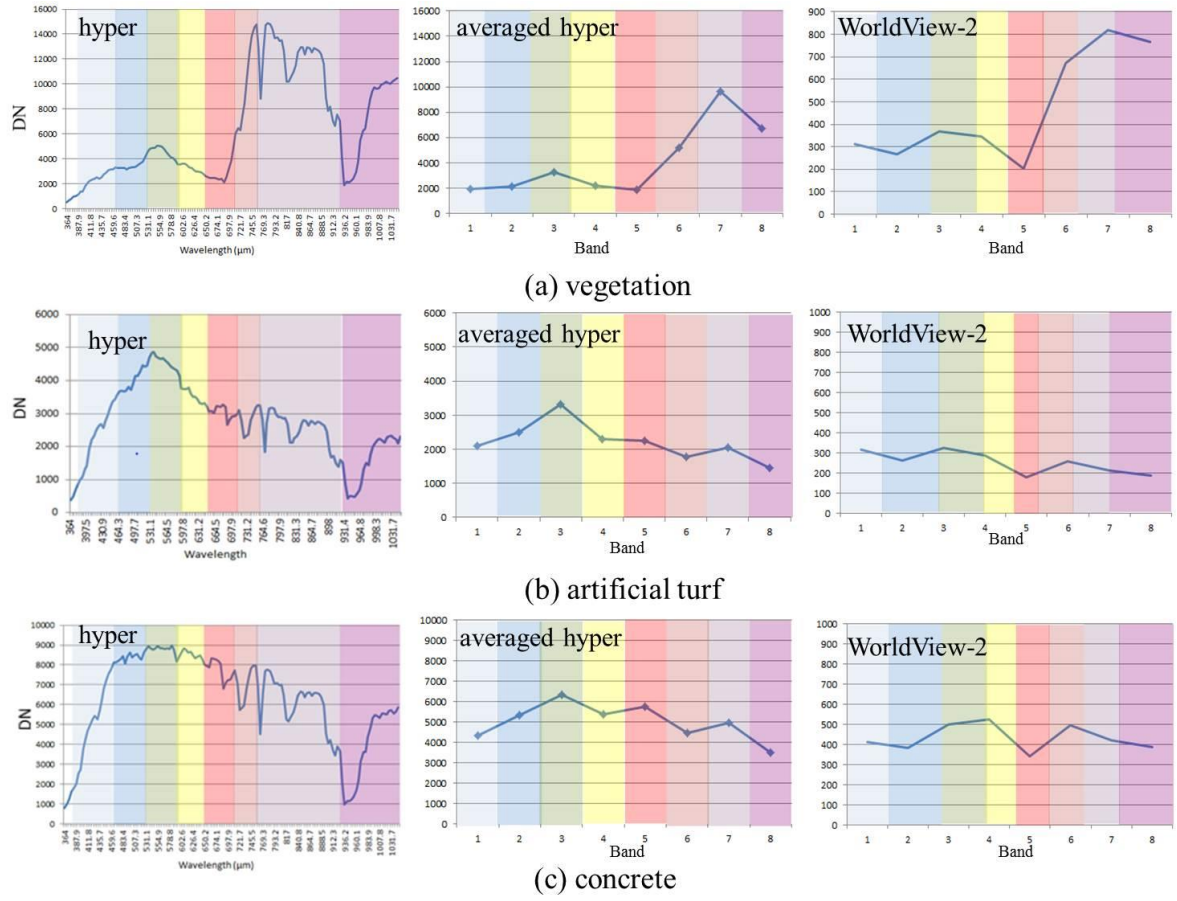

Figure 7. Comparison of hyperspectral, averaged-hyperspectral, and multispectral data for the three surface materials (a: lawn, b: artificial turf, c: concrete) shown in Figure 5

Next, the comparison between the DN values from the airborne HS sensor (CASI-1500) and the satellite (WV-2) MS sensor was carried out. Because the HS data include as many as 144 bands, the DN values of these bands were averaged and converted to 8-band DN values corresponding to WV-2 sensor (i.e. Coastal, Blue, Green, Yellow, Red, Red Edge, NIR1, NIR2) for comparison. The average digital number for the corresponding band *i* of WV-2 is calculated by Eq. (1) as

$$\overline{DN_i} = \sum_{k_i} DN(\lambda_{k_i}) R_e(\lambda_{k_i}) \,/\, \sum_{k_i} R_e\,(\lambda_{k_i}) \tag{1}$$

where $DN(\lambda)$ is the observed digital number from the HS sensor at wavelength λ, $R_e(\lambda)$ is the relative spectral radiance response value of WV-2 in **Figure 3**, k_i is the effective HS band numbers for WV-2's band *i* whose $R_e(\lambda)$ value is larger than 0.001.

The averaged HS's DN value for each surface material looks to have a similar shape as that from the MS sensor. Since the WV-2 data are presented by 11 bits (0 - 2047) as in Ref. [11] while the dynamic range of CASI-1500 is 14-bits (0 - 16383) as in Ref. [9], the absolute value of their DN ratio has only relative meaning. The DN ratios for the three materials are compared in **Figure 8**. Although

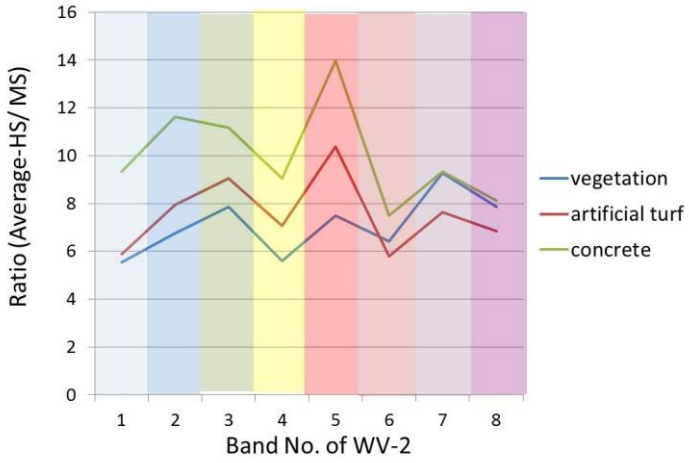

Figure 8. Comparison of the ratio between averaged-HS data and MS data for the three surface materials (a: lawn, b: artificial turf, c: concrete), shown in Figure 7

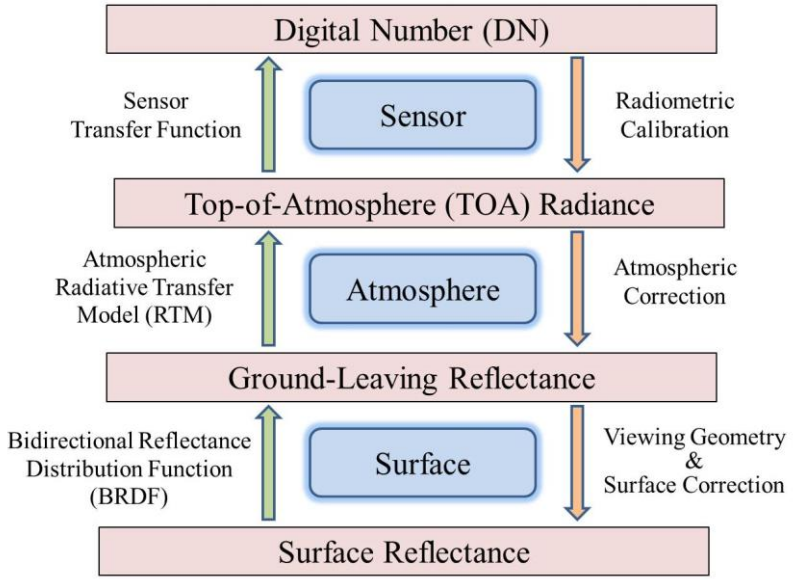

Figure 9. Spectral characterization of hyperspectral remote sensing data [5]

some differnces are seen, the DN ratio is basically in a similar value for different bands and materials. The differences in the HS and MS data used in this study can be explained by **Figure 9**. The systematic difference between them is the effects of atmospher; the MS data corresponds to the Top-of-Atmosphere (TOA) radiance while the HS data to the Middle-of-Atmosphere (MOA) radiance. Other differences, such as the acquisition date and time, and resulting sunlight and air conditions, viewing geometry, and image resolution, also exist. In spite of these differences, the averaged HS data here are still almost comparable with the MS data.

After observing spectral characteristics of various surface materials of the HS image, training data for preliminary supervised classification were selected as shown in **Figure 10** (a). Due to the very high dimensionality of the HS data, the standard maximum likelihood classifier (MLC) was difficult to apply. A principal component analysis (PCA) reduces such a high-dimensional problem to a much lower-dimensional one owing to the similarity of neighboring HS bands.

In this study, however, a simple Nearest Neighbor (NN) classification was carried out using all the 144 HS bands as a first attempt. The results of the NN classification for the HS and MS images are compared in **Figure 10**. Due to the limited number of training classes, the results look similar although some differences can be seen in roofs. We will try more sophisticated classification methods in the near future and reveal the effectiveness of HS data in urban land cover classification.

(a) Training data

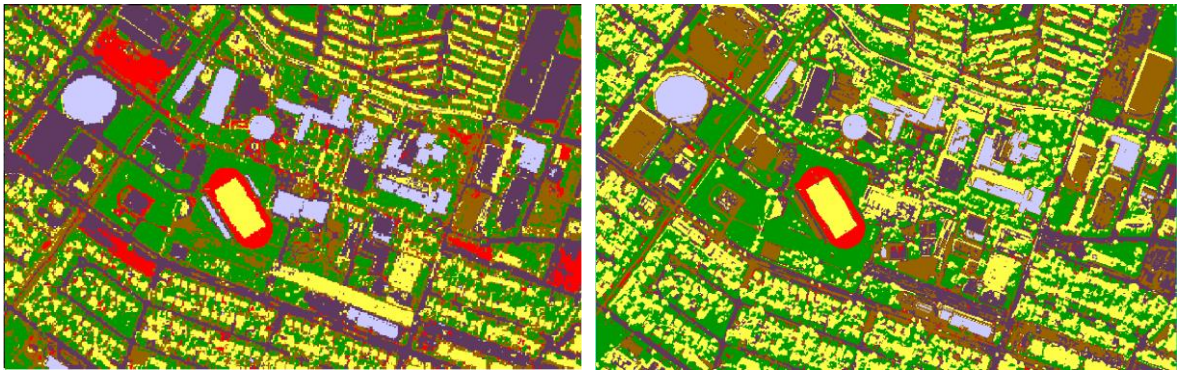

(b) Hyperspectral (HS) image (c) Multispectral (MS) image

Figure 10. Supervised classification for the HS and MS images. (a) Training data used for

CONCLUSIONS

Using airborne hyperspectral (HS) data acquired by CASI-1500 imager over Houston, Texas, USA, the spectral reflectance characteristics of surface materials were investigated. The HS data include 144 spectral bands in the visible to near-infrared (380 nm to 1050 nm) regions. A multispectral (MS) image acquired by WorldView-2 satellite was also introduced in order to compare it with the HS image. A field measurement was also carried out using a handheld spectroradiometer by the authors. The irradiances of surface materials obtained by the measurement were also compared with the digital

numbers of the HS data and they showed a reasonable level of agreement. Finally supervised classification was conducted for the HS and MS data and their results were discussed. Although our study is still preliminary, the results of more detailed investigation will be presented in the near future.

ACKNOWLEDGMENT

The hyperspectral data used in this study were provided from the 2013 IEEE Geoscience and Remote Sensing Society Data Fusion Contest.

REFERENCES

[1] Rathje, E., and Adams, B.J., 2008, The role of remote sensing in earthquake science and engineering, opportunities and challenges, *Earthquake Spectra*, 24(2), 471–492.

[2] Eguchi, R.T., Huyck, C., Ghosh, S., Adams, B.J., 2008, The application of remote sensing technologies for disaster management, *The 14th World Conference on Earthquake Engineering*, CD-ROM, 17p.

[3] Brunner, D., Lemoine, G., and Bruzzone, L., 2010, Earthquake damage assessment of buildings using VHR optical and SAR imagery, *IEEE Transactions on Geoscience and Remote Sensing*, 48(5), 2403-2420.

[4] Meslem, A., Yamazaki, F., Maruyama, Y., 2011, Accurate evaluation of building damage in the 2003 Boumerdes, Algeria earthquake from QuickBird satellite images, *Journal of Earthquake and Tsunami*, 5(1), 1-18.

[5] Bioucas-Dias, J.M., Plaza, A., Camps-Valls, G., Scheunders, P., Nasrabadi, N.M., Chanussot, J., 2013, Hyperspectral remote sensing data analysis and future challenges, *IEEE Geoscience and Remote Sensing Magazine*, 1(2), 6-36.

[6] MicroImages, Inc., 2012, Introduction to hyperspecral imaging, Available online: http://www.microimages.com/documentation/Tutorials/hyprspec.pdf (accessed on 14th September 2013).

[7] Pompilio, L., Villa, P., Boschetti, M., Pepe, M., 2013, Spectroradiometric field surveys in remote sensing practice: a workflow proposal, from planning to analysis, *IEEE Geoscience and Remote Sensing Magazine*, 1(2), 37-51.

[8] 2013 IEEE GRSS Data Fusion Contest, 2013, Fusion of Hyperspectral and LiDAR Data, Available online: http://www.grss-ieee.org/community/technical-committees/data-fusion/data-fusion-contest/ (accessed on 14th September 2013).

[9] ITRES Research Limited, 2011, CASI-1500 Hyperspectral Imager, Available online: http://www.itres.com/products/imagers/casi1500/ (accessed on 14th September 2013).

[10] ITRES Research Limited, 2006, Operations and Mission Planning for ITRES' CASI 1500h system, Available online: ftp://snr-0563.unl.edu/Incoming/For_Rick/CASItraining/CASI_1500h_System_Op_Training.ppt (accessed on 14th September 2013).

[11] DigitalGlobe, Inc., 2010, Radiometric Use of WorldView-2 Imagery: Technical Note, Available online:http://www.digitalglobe.com/sites/default/files/Radiometric_Use_of_WorldView-2_Imagery%20(1).pdf (accessed on 14th September 2013).

[12] EKO Instruments Co., 2013, MS-720 Spectroradiometer, Available online: http://eko-eu.com/products/solar-radiation-and-photonic-sensors/spectroradiometers/ms-720-spectroradiometer (accessed on 14th September 2013).

[13] Yamazaki, F., Matsuoka, M., Warnitchai, P., Polngam, S., Ghosh, S., 2005, Tsunami Reconnaissance Survey in Thailand Using Satellite Images and GPS, *Asian Journal of Geoinformatics*, 5(2), 53-61.

[14] Liu, W., Yamazaki, F., 2012, Object-based shadow extraction and correction of high-resolution optical satellite images, *IEEE Journal of Selected Topics in Applied Earth Observations and Remote Sensing*, DOI: 10.1109/JSTARS.2012.2189558, 5(4). 1296-1302.